J Mol Model (2012) 18:3291–3300
DOI 10.1007/s00894-011-1341-8

ORIGINAL PAPER

Self-assembly of DNA on a gapped carbon nanotube

Alfredo D. Bobadilla · Jorge M. Seminario

Received: 4 September 2011 / Accepted: 19 December 2011 / Published online: 18 January 2012

Abstract We perform molecular dynamics simulations to analyze the wrapping process of a single-stranded (ss) DNA around a gapped CNT immersed in a bath of water. We observe the formation of a stable molecular junction with the ssDNA adopting a helical or circular conformation around one CNT electrode and a linear conformation around the opposite electrode. We find that DNA undergoes several conformational changes during equilibration of the self-assembled molecular junction. This process would allow a higher yield of successful CNT-DNA interconnections, which constitutes a novel structure of interest in chemical and biological sensing at the single-molecule level.

Keywords Carbon nanotube · DNA · Hybrid nanostructures · Molecular junction · Self-assembly

Introduction

Biological molecules integrated in nanosensors offer novel possibilities to reach a higher degree of chemical sensitivity and specificity due to the variety on structure-function and molecular recognition mechanisms of molecules in the living cell. Specifically, DNA has been investigated recently in several nanotechnology applications [1–20]. On the other hand, carbon nanotubes (CNT) are suitable as molecular interfaces due to their unique electrical conductivity and mechanical stiffness [1, 21–30] as well as due to the possibility to manipulate their structure and function through oxidative processes using ion or electron beams [31].

DNA base-pair recognition properties allow us to make arbitrary DNA-based nanostructures [32–34] and some efforts on the electrical characterization of these nanostructures have already been performed [35, 36]. DNA-CNT interactions in water solution show self-assembly properties [37], which can be exploited for making hybrid nanodevices [38–41] and be combined with other molecular electronics approaches [42–47].

Molecular imaging instruments such as scanning electron microscope (SEM) and atomic force microscope (AFM) do not allow getting details at the atomistic level and they have limitations on imaging suspended nanostructures. On the other hand, molecular dynamics simulations allow the analysis and prediction of structural conformations of CNT wrapped by DNA [48, 49]. For instance Zheng et al. [50] proposed, based on AFM measurements, that poly GT (sequences of repeating guanine and thymine nucleotides) wraps helically around CNT as a hydrogen-bonded dimer with a 18 nm pitch helix. However using molecular dynamics simulations, Johnson et al. [48] found that an 18 nm pitch helical wrapping is structurally unstable, but a helical conformation with denser pitch was strongly favored and hybridization between multiple adsorbed poly GT oligonucleotides was unfavorable due to geometric factors.

A. D. Bobadilla · J. M. Seminario (✉)
Department of Chemical Engineering,
Texas A&M University College Station,
Texas 77843, USA
e-mail: seminario@tamu.edu

A. D. Bobadilla · J. M. Seminario
Department of Electrical and Computer Engineering,
Texas A&M University, College Station,
Texas 77843, USA

J. M. Seminario
Materials Science and Engineering Graduate Program,
Texas A&M University, College Station,
Texas 77843, USA

Table 1 Lennard-Jones and Coulombic interactions are computed with an additional switching function S(r) detailed in Eq. 3

Cutoff	Lennard Jones	Coulombic
$r < r_{in}$	$V_{L\_J}(r)$	C(r)
$r_{in} < r < r_{out}$	$S(r) \times V_{L\_J}(r)$	$S(r) \times C(r)$
$r > r_{out}$	0	0

Guo et al. [51] developed a method to connect a carbon nanotube gap with single DNA molecule. In their method, amine functionalization of DNA molecules allowed the covalent amide linkage to CNT functionalized with carboxyl groups; they obtained ten working devices out of 370 that were tested. This low yield on successful interconnection of carbon nanotube with DNA is due to an inherent difficulty on creating a covalent bond. In the present work, a self-assembly process is analyzed in which a single stranded DNA molecule bridges a gapped CNT through noncovalent bonding.

Methods

The molecular system under study consists of a single stranded (ss) DNA molecule with an initial helical conformation positioned parallel to a single-walled CNT. The initial separation between DNA and CNT is 15 Å, and the nanotube gap is 22 Å (Fig. 3a). Two types of carbon nanotube are considered in the analysis of CNT-DNA assembly, the (4,0) and (5,0) CNTs. By making terminal carbon atoms to share a covalent bond, we get a CNT structure periodic along the z-direction. The simulation box size is 40Å × 50Å × 80Å and includes 4500 TIP3P water molecules as well as 14 Na^+ counterions to exactly neutralize the negatively charged ssDNA backbone. The software PACKMOL [52] is used to construct the initial configuration of the system.

The dynamics of the system is modeled with the CHARMM force field [53] included in the large-scale atomic/molecular massively parallel simulator (LAMMPS) program [54]. Periodic boundary conditions are applied to a canonical NVE ensemble. Electrostatic interactions are calculated by the particle-particle and particle-mesh (PPPM) [55] method using a precision of 10^{-4}. CNTs are modeled as uncharged Lennard-Jones particles using sp^2 carbon parameters from the CHARMM force field. To control the temperature, atom velocities are rescaled at every time-step by using the Berendsen thermostat [56], which is applied to only the translational degrees of freedom. The positions of all CNT atoms are constrained by not updating the velocity for atoms in the CNT, as expected applications consider the CNT attached to fixed metal electrodes. Visualization of trajectories is performed using the Visual Molecular Dynamics (VMD) software [57]. van der Waals energy corresponding to CNT interactions with the ssDNA, and

Table 2 Pair coefficients epsilon (ε) and sigma (σ) for interactions between atoms of the same type (Fig. 1). (Units: kcal/mol and Å, respectively)

Atom type	ε	σ	Atom label	Atom type	E	σ	Atom label
1	0.110	3.563595	C	21	0.028	2.387609	HN8
2	0.100	3.385415	CN1	22	0.024	2.387609	HN9
3	0.100	3.385415	CN1T	23	0.200	3.296325	NN1
4	0.100	3.385415	CN2	24	0.200	3.296325	NN2
5	0.090	3.385415	CN3	25	0.200	3.296325	NN2B
6	0.090	3.385415	CN3T	26	0.200	3.296325	NN2U
7	0.075	3.385415	CN4	27	0.200	3.296325	NN2G
8	0.075	3.385415	CN5	28	0.200	3.296325	NN3
9	0.075	3.385415	CN5G	29	0.200	3.296325	NN3A
10	0.020	4.053589	CN7	30	0.200	3.296325	NN3G
11	0.020	4.053589	CN7B	31	0.200	3.296325	NN4
12	0.056	3.581413	CN8	32	0.1521	3.150574	OT
13	0.056	3.581413	CN8B	33	0.1200	3.029056	ON1
14	0.078	3.634867	CN9	34	0.1200	3.029056	ON1C
15	0.046	0.400014	HT	35	0.1521	3.153781	ON2
16	0.046	0.400014	HN1	36	0.1200	3.029056	ON3
17	0.046	0.400014	HN2	37	0.1521	3.153781	ON5
18	0.046	1.959977	HN3	38	0.1521	3.153781	ON6
19	0.046	0.400014	HN5	39	0.5850	3.830864	P
20	0.022	2.351973	HN7	40	0.0469	2.429926	SOD

coulombic energy corresponding to interactions between adjacent phosphate atoms in the ssDNA backbone are computed as defined in the CHARMM force field (Table 1).

Previous to every molecular dynamics simulation, an energy minimization of the system is performed to reach a local potential energy minimum to avoid hot spots. Then the temperature of the system is raised from 5 K to 300 K in a 0.5 ns run using a 2 fs time step; this time step is used in all cases. Then a 1 ns run at 300 K is performed to ensure equilibration. To accelerate the wrapping process, the temperature is raised to 330 K in a 1 ns run, and the system is allowed to equilibrate at 330 K for 42 ns, until the average root mean square deviation (avRMSD) was observed to stabilize with a deviation of less than 0.05 Å within a nanosecond of simulation time. The RMSD is calculated for the DNA structure with respect to its initial conformation according to Eqs. 7 and 8.

The Lennard-Jones potential,

$$V_{LJ}(r) = 4 \in \left[\left(\frac{\sigma}{r}\right)^{12} - \left(\frac{\sigma}{r}\right)^{6}\right] \quad (1)$$

represents nonbonded interactions between pairs of atoms separated by at least three bonds. It is composed of two terms:

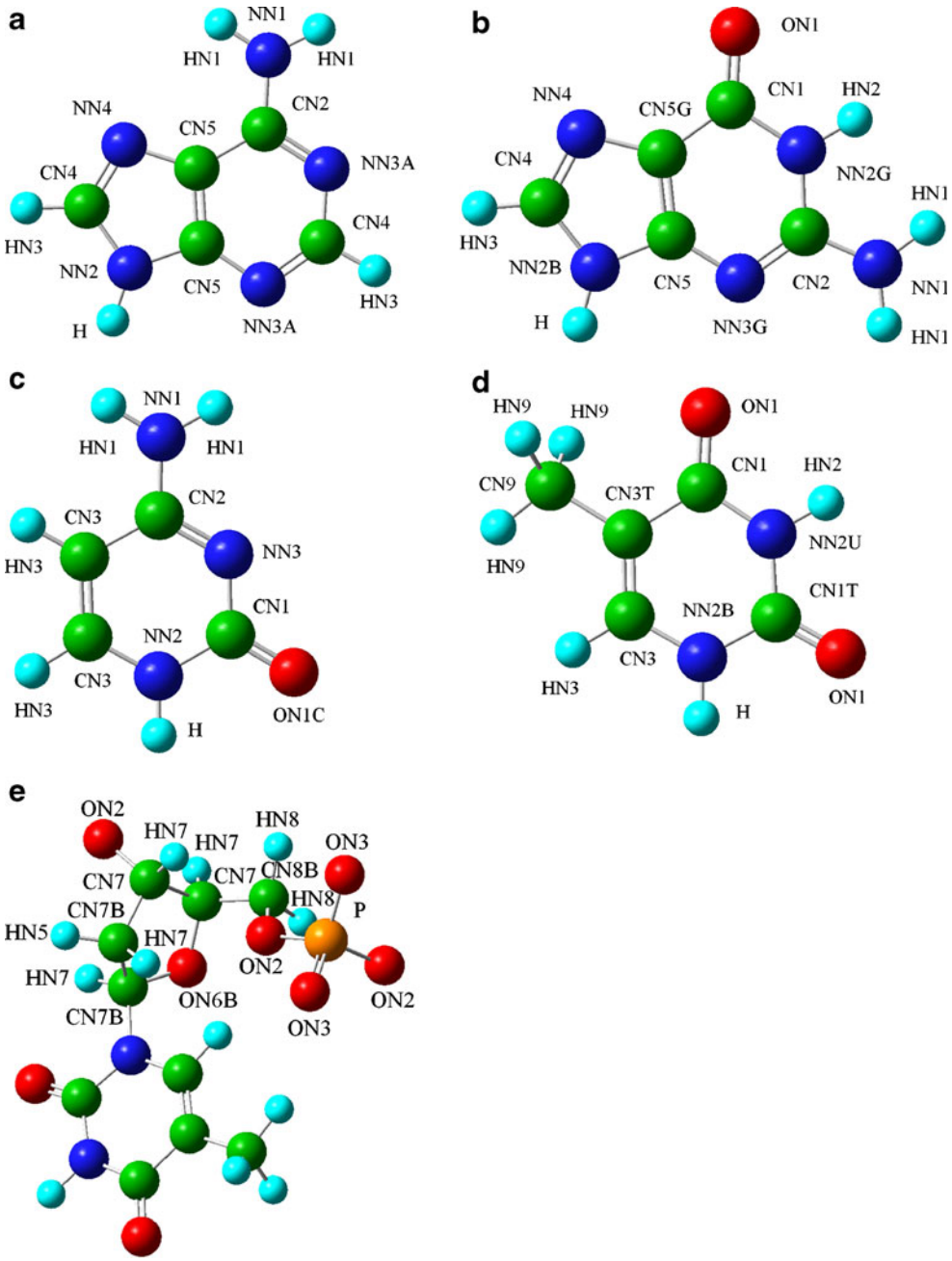

Fig. 1 Structures and atom labels for (a) adenine, (b) guanine, (c) cytosine, (d) thymine, (e) sugar and phosphate groups

the first describes the Pauli repulsive interaction at short ranges due to overlapping electron orbitals, and the second describes the van der Waals attractive interaction at long ranges due to dipole-dipole interactions and to fluctuating molecular dipole moments. Table 2 shows the pair interactions coefficients between atoms of the same kind (Fig. 1).

The Coulombic potential,

$$C(r) = \frac{Cq_i q_i}{\varepsilon r} \tag{2}$$

represents interactions between static atomic charges. Lennard-Jones and Coulombic interactions are computed with an additional switching function S(r),

$$S(r) = \frac{\left[r_{out}^2 - r^2\right]^2}{\left[r_{out}^2 - r_{in}^2\right]^3}\left[r_{out}^2 + 2r^2 - 3r_{in}^2\right], \tag{3}$$

which allows decreasing interaction energies smoothly when the interatomic distance is larger than an inner cutoff, and forcing the energies to zero if the interatomic distance exceeds an outer cutoff distance.

We use inner and outer cutoff values of r_{in}=8 Å and r_{out} =10 Å, respectively, for Lenard-Jones and Coulombic nonbonded interactions.

For interactions between atoms of different type, pair coefficients, ε and σ, are determined according to the following mixing rules,

$$\in_{ij} = \sqrt{\in_i \times \in_j} \tag{4}$$

and

$$\sigma_{ij} = \frac{\sigma_i + \sigma_j}{2} \tag{5}$$

where, *i* and *j* correspond to the atom types shown in Table 2.

To quantify torsional interactions, ssDNA backbone dihedral angles (Fig. 2) are also computed according to Eq. 6.

$$\tau = 2\pi + a\tan 2(|v2|v1.[v2 \times v3], [v1 \times v2].[v2 \times v3]) \tag{6}$$

To analyze changes in the DNA structure as a whole, we compute the root mean square deviation (RMSD) of atomic coordinates averaged over the entire simulation, which indicates the average scalar distance between atoms of the same type for ssDNA with respect to its initial structure, allowing one to assess how well the DNA structure is maintained during the simulation:

$$RMSD(i) = \sqrt{\frac{\Sigma_k^M |r_{ik} - r_{0k}|^2}{M}}, \tag{7}$$

where the summation runs over all the M atom positions in the DNA molecule at the ith snapshot. Finally the average RMSD through the snapshots is calculated from

$$avRMSD(N) = \frac{\Sigma_i^N RMSD(i)}{N} \tag{8}$$

where the summation runs over N snapshots of the simulation.

Results

Simulations are performed to analyze the interaction of a gapped single-walled carbon nanotube (CNT), interacting with a 15-base ssDNA molecule. The gap in the CNT divides the CNT in left and right (branches) CNTs that eventually may serve as electrodes in practical applications. The self-assembly of the molecular junction is driven by a strong van der Waals attraction between the faces of the nucleobases and the CNT sidewall.

A 15-base ($A_1T_1C_1A_2A_3T_2A_4T_3C_2C_3A_5C_4C_5T_4G$) ssDNA, chosen at random, is initially at 1.5 nm from the gapped CNT (Fig. 3a). During the initial process, when increasing temperature from 5K to 330K (Figs. 3a, 3b, 3c

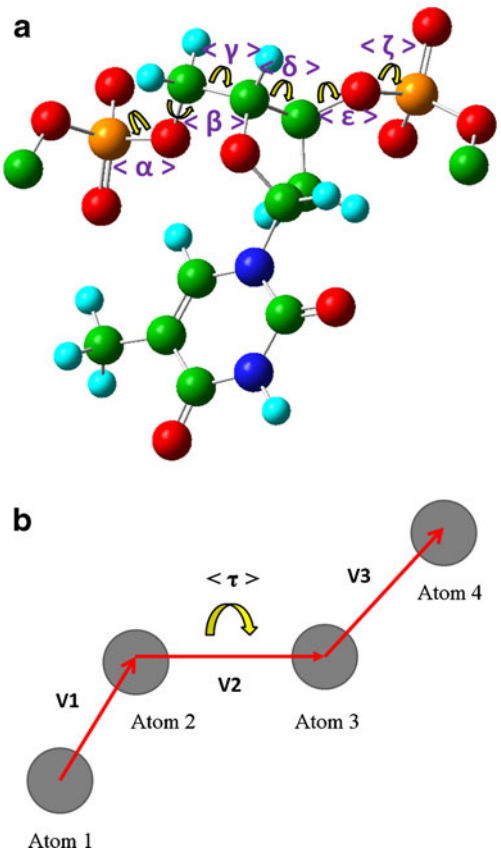

Fig. 2 (a) Dihedral angles in DNA backbone. (b) Definition of the dihedral angle τ

and 3d), the DNA molecule approaches the CNTs (4,0) filling the gap; in this process, the DNA molecule elongates losing its helical-stacked conformation. After 8 ns of equilibration, at 330 K (Fig. 3e), the ssDNA molecule adopts a linear conformation along the left CNT electrode and the ($C_4C_5T_4G$) segment adopts a loop conformation on the right electrode due to stacking of cytosine (C_4) and guanine (G). Additional 8 ns of equilibration at 330K is required to observe a clear helical wrapping process (Fig. 3f), adopting ssDNA a helical conformation around one CNT electrode and a linear conformation on the opposite CNT electrode, with four DNA bases filling the gap and only three bases on the right CNT electrode. Further equilibration at 330K is performed, after which we observe the ssDNA structural conformation changes from helical to circular (Fig. 3g), with only three DNA bases filling the gap and five bases on the right CNT electrode. The adoption of circular conformation in the DNA segment ($A_1T_1CA_2A_3T_2$) is aided by the formation of a hydrogen bond between adenine (A_1) and thymine (T_2) bases; this bond formation is promoted by the high temperature (330K) imposed to the system. The ssDNA circular conformation is stable for 18 ns at 330K (Figs. 3g,h,i), after which we observe the final stable conformation adopted by ssDNA. This is a circular conformation on one CNT electrode and a loop ($C_4C_5T_4G$) on the opposite electrode (Fig. 3i); the loop structure is due to formation of hydrogen bond between cytosine (C_4) and guanine (G). Figure 4 shows a similar evolution for ssDNA wrapping around a gapped CNT(5,0).

However, there is a difference between the DNA wrapping processes for the CNT(4,0) and CNT(5,0). For interaction of ssDNA with CNT(4,0), we observe that the DNA molecule stabilizes slowly on the CNT surface, adopting at room temperature, a linear conformation on the left

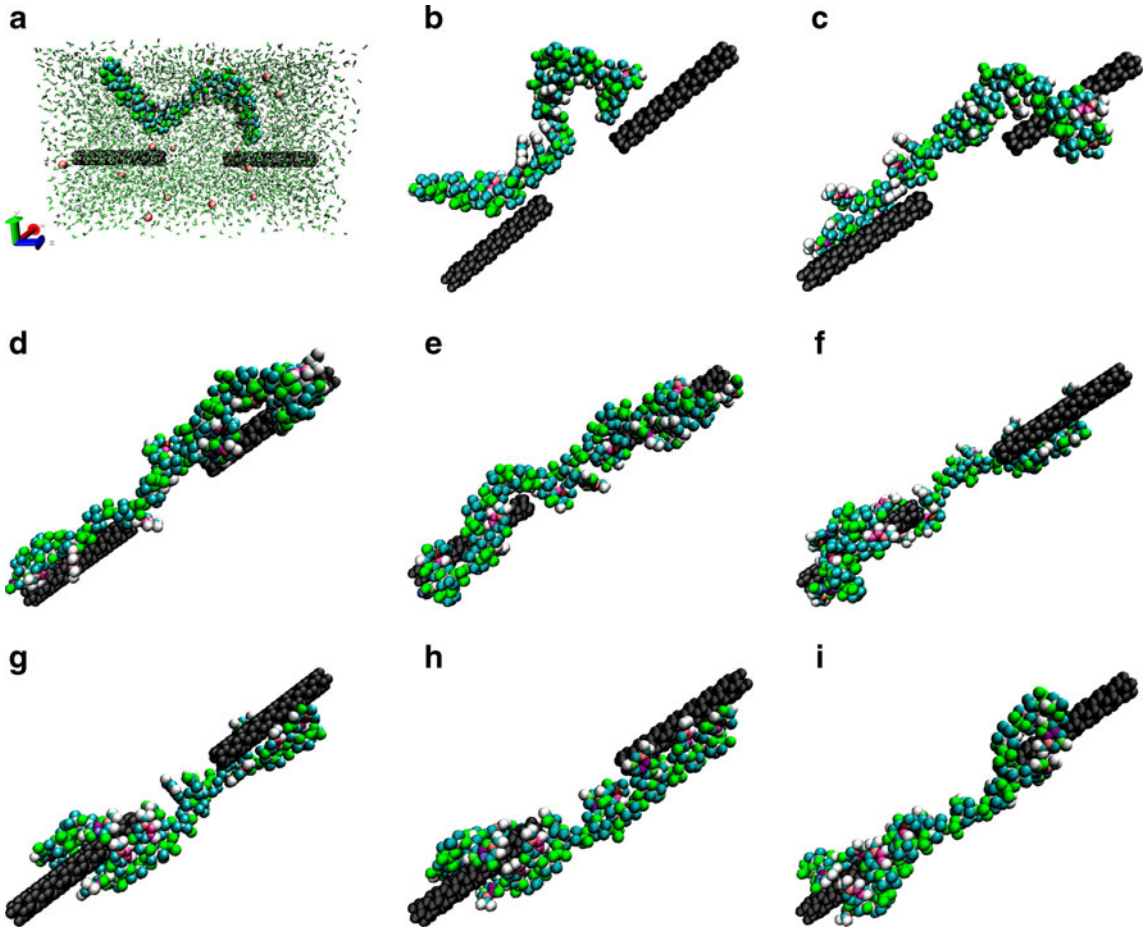

Fig. 3 Time evolution of ssDNA ($A_1T_1C_1A_2A_3T_2A_4T_3C_2C_3A_5C_4C_5T_4G$) structural conformation around CNT (4,0). (a) t=0 ns, T=0 K, initial configuration for the system. (b) t=0.5 ns, T=300K, ssDNA begin to approach CNT. (c) t=1.5 ns, T=300K, tendency for a wrapping process. (d) t=2.5 ns, T=330K, ssDNA gets elongated along CNT. (e) t=10.5 ns, T =330K, beginning of wrapping process. (f) t=18.5 ns, T=330K, ssDNA adopts helical conformation on one of the CNT branches and loop conformation on the opposite one. (g) t=26.5 ns, T=330K, formation of hydrogen bond between adenine (A_1) and thymine (T_2) bases causes ssDNA changing conformation from helical to circular. (h) t=34.5 ns, T=330K, ssDNA keeps the same structural conformation. (i) t=44.5 ns, T=300K, ssDNA changes from linear conformation to loop conformation on the right CNT electrode, aided by the formation of a hydrogen bond between cytosine (C_4) and guanine (G)

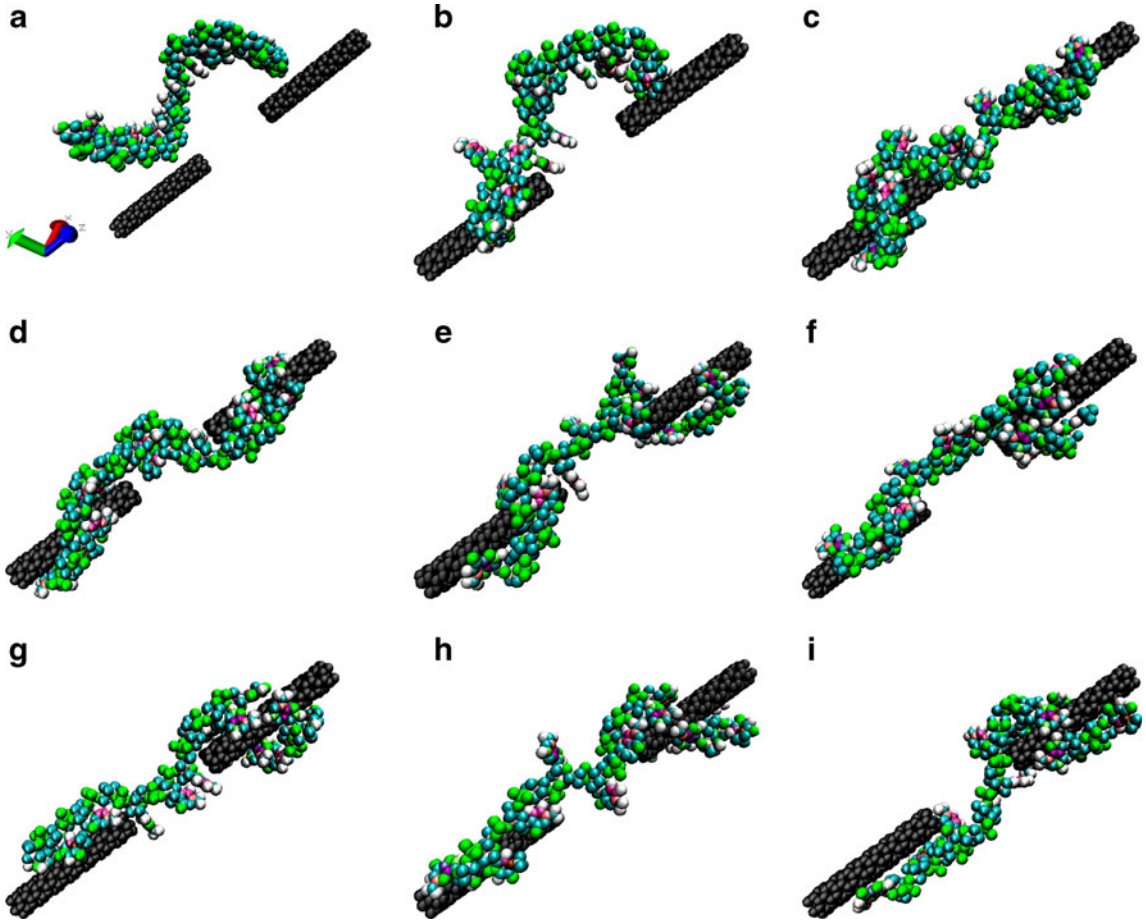

Fig. 4 Time evolution of the ssDNA ($A_1T_1C_1A_2A_3T_2A_4T_3C_2$-$C_3A_5C_4C_5T_4G$) structural conformation around CNT (5,0). (a) t=0 ns, T=0 K, initial configuration for the system. (b) t=1 ns, T=300K, ssDNA begins to approach CNT. (c) t=1.5 ns, T=300K, , ssDNA adopts helical conformation on one CNT branch and a linear conformation on the opposite. (d) t=2.5 ns, T=330K; ssDNA keeps same structural conformation. (e) t=10.5 ns, T =330K, ssDNA adopts a helical conformation on both CNT branches, (f) t=18.5 ns, T=330K; ssDNA adopts circular conformation on one CNT, aided by the formation of a hydrogen bond between cytosine (C_2) and guanine (G), and a linear conformation on the opposite branch. (g) t=26.5 ns, T=330K, a new hydrogen bond is formed between thymine (T_3) and adenine (A_5), contributing to the stability of the ssDNA circular conformation. Only two bases are on the left CNT electrode and four bases filling the CNT gap. (h) t=34.5 ns, T=330K; ssDNA keeps same structural conformation. (i) t=44.5 ns, T=300K, ssDNA keeps same structural conformation

electrode and a helical but stacked conformation on the right electrode (Fig. 3c), with stacking of two DNA bases. While for the interaction of ssDNA with CNT(5,0), we observe the DNA molecule approaches the CNT surface faster, adopting the ssDNA a helical conformation on the left electrode at room temperature (Fig. 4c), with DNA bases stacked to the CNT surface.

We notice that the magnitude of van der Waals (vdW) interaction energy between CNT and DNA is stronger for the CNT(5,0) case (Fig. 6b) compared to the CNT(4,0) case (Fig. 5b) and the oscillation of van der Waals energy is smaller for the CNT(5,0) case; this is due to a higher surface area on the CNT(5,0). We also observe that the vdW energy decreases notoriously at the beginning of the equilibration steps at 300K (time=0.5 ns) and at 330K (time=2.5 ns) due to the wrapping of ssDNA around CNT surface.

A general mechanism of the wrapping process of ssDNA around carbon nanotube occurs from the 3' end to the 5' end [48]. In the present work the (4,0) and (5,0) CNTs are considered for the analysis of the interaction with the ssDNA and we observe in both cases a wrapping process from the 3' end to the 5' end. For the CNT (4,0), the ssDNA wraps the carbon nanotube adopting a circular conformation on the left electrode (Fig. 3i, Table 3); however, for the CNT(5,0) case, ssDNA adopts a circular conformation on the right CNT electrode (Fig. 4i, Table 4).

The mechanism responsible for the ssDNA overall structural conformation is credited to electrostatic and torsional interactions within the sugar-phosphate backbone because the backbone contains an intrinsic curvature and prefers a helical wrapping rather than a linear one. A decrease in

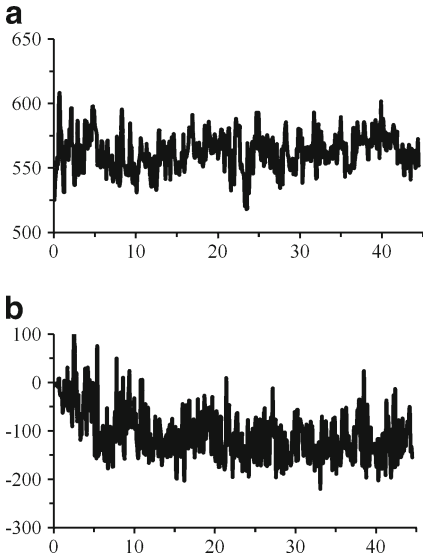

Fig. 5 Time evolution of (a) electrostatic energy of interaction between adjacent phosphate atoms and (b) van der Waals energy of interaction between the CNT(4,0) and the ssDNA molecule. Energy units are in kcal mol^{-1} and time in ns

electrostatic energy during the first 10 ns of simulation time (Figs. 5a, 6a) is associated with an increase in phosphate-phosphate distance in the DNA backbone and a corresponding decrease in electrostatic repulsion, favoring a helical conformation for ssDNA. Structural and energetic changes in ssDNA proceed via a rearrangement of the average torsional angles $< \tau >$ (Fig. 2) in the ssDNA backbone (Fig. 7).

We denote by avRMSD (Fig. 8) the RMSD value averaged over the simulation time, stopping the simulation when the avRMSD is observed to stabilize with a deviation not bigger than 0.05 Å within a nanosecond of simulation time (Table 5).

We also observe a tendency for a helical conformation in ssDNA structure during the equilibration process at 330K, nevertheless, helical turns continue being generated, forcing the ssDNA conformation to change from the helical to a circular one, aided by the formation of hydrogen bonds. The final stable conformation of ssDNA is a circular one on one electrode and a linear or loop conformation on the opposite CNT electrode; both h-bonded conformations are shown in

Table 3 Time evolution of ssDNA structural conformations around CNT (4,0)

Time (ns)	Temperature (K)	ssDNA conformation		Energy (kcal/mol)	
		Left CNT	Right CNT	Coulombic	vdW
1.5	300	Linear	Helical	570.9	-47.2
2.5	330	Linear	Helical	536.9	110.7
10.5	330	Linear	Loop	559.7	-155.7
18.5	330	Helical	Linear	556.9	-141.5
26.5	330	Circular	Linear	557.1	-172.1
34.5	330	Circular	Linear	553.5	-83.8
44.5	330	Circular	Loop	551.8	-154.1

Table 4 Time evolution of ssDNA structural conformations around CNT (5,0)

Time (ns)	Temperature (K)	ssDNA conformation		Energy (kcal/mol)	
		Left CNT	Right CNT	Coulombic	vdW
1.5	300	Helical	Linear	603.5	-147.9
2.5	330	Helical	Linear	601.6	-146.1
10.5	330	Helical	Helical	548.2	-193.3
18.5	330	Linear	Circular	587.9	-184.7
26.5	330	Linear	Circular	588.3	-180.1
34.5	330	Linear	Circular	587.6	-183.9
44.5	330	Linear	Circular	594.6	-188.0

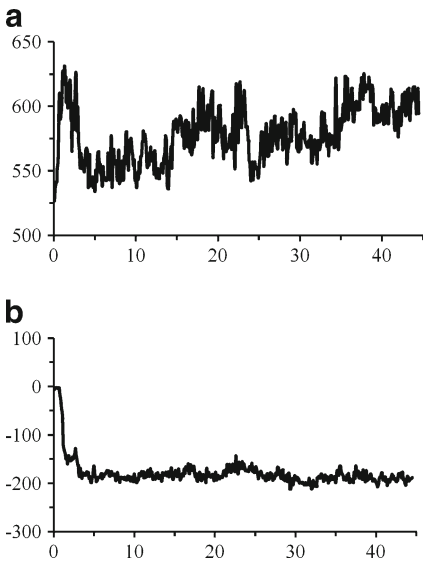

Fig. 6 Time evolution of (a) electrostatic energy of interaction between adjacent phosphate atoms and (b) van der Waals energy of interaction between single-walled carbon nanotube (5,0) and the ssDNA molecule. Energy units are in kcal mol^{-1} and time in ns

Figs. 4g,i and 5f,g. When the circle forms on one end of the ssDNA, the other end is no longer able to adopt a helix shape because the remaining ssDNA is not long enough. In other trials with several initial configurations, DNA forms loops and disordered kinked structures because of steric interactions between adjacent bases and the ssDNA flexibility, being a polymer with several degrees of freedom, yielding a very irregular energy landscape with several local minima [49].

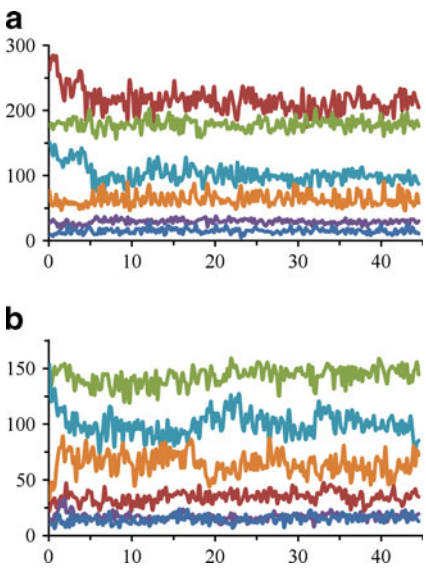

Fig. 7 Time evolution of average ssDNA dihedral angles $< \tau >$ (°) for (a) ssDNA-CNT(4,0) and (b) ssDNA-CNT(5,0) molecular junctions. Time is in ns and curves are color coded: alpha (red), beta (green), epsilon (turquoise), gamma (orange), delta (purple), zeta (blue)

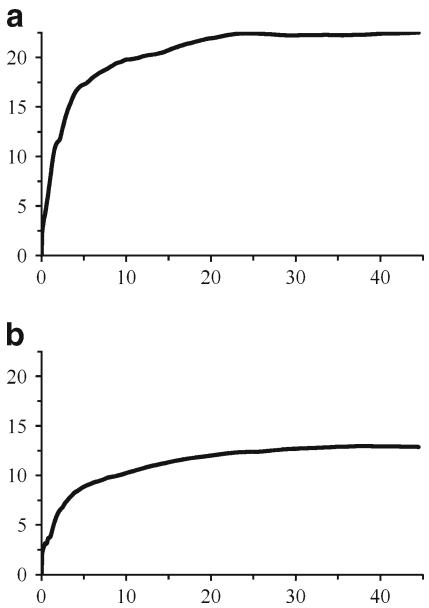

Fig. 8 Time (nanoseconds) evolution of averaged root mean square deviation (avRMSD, in Å) calculated for the ssDNA molecule with respect to its initial conformation. Plots correspond to (a) ssDNA-CNT(4,0) and (b) ssDNA-CNT(5,0)

Conclusions

Atomistic molecular dynamics simulations have been performed exploring the self-assembly dynamics and structure of a molecular junction enabled by the CNT-DNA wrapping process. ssDNA is able to bridge a carbon nanotube gap adopting different structural configurations around each carbon nanotube, a helical configuration and then a circular conformation around one CNT branch during the equilibration process at 330K; this conformation is kept at room temperature; while on the other CNT, ssDNA adopts a linear elongated or otherwise loop configuration during the process at 330K and keeps that conformation at room temperature. We attribute the different conformations DNA adopts in our molecular junction to the influence of mainly two factors, length of ssDNA on each CNT electrode and the arrangement of hydrogen bonds on the CNT surface.

Table 5 Summary of avRMSD values for ssDNA during the last 5 ns of simulation

Time (ns)	avRMSD (Å)	
	ssDNA-CNT(4,0)	ssDNA-CNT(5,0)
40.5	22.42	12.95
41.5	22.43	12.94
42.5	22.45	12.93
43.5	22.48	12.92
44.5	22.48	12.90

Acknowledgments This research was supported by the U.S. Defense Threat Reduction Agency (DTRA) through the U. S. Army Research Office (ARO) under grant number W911NF-06-1-0231, the ARO under a Defense University Research Instrumentation Program (DURIP) project number # W91NF-07-1-0199 and under a Multidisciplinary University Research Initiative (MURI) Project # W911NF-11-1-0024. We also acknowledge the Texas A&M Supercomputing Facility, where part of the calculations were performed.

References

1. Katz E, Willner I (2004) Biomolecule-functionalized carbon nanotubes: applications in nanobioelectronics. Chem Phys Chem 5:1084–1104
2. Bergeron F, Houde D, Hunting DJ, Wagner JR (2004) Electron transfer in DNA duplexes containing 2-methyl-1,4-naphthoquinone. Nucl Acids Res 32:6154–6163
3. Woolard D, Globus T, Gelmont B, Bykhovskaia M, Samuels A, Cookmeyer D, Hesler J, Crowe T, Jensen J, Jensen J et al (2002) Submilimeter-wave phonon modes in DNA macromolecules. Phys Rev E 65:051903. doi:10.1103/PhysRevE.65.051903
4. Fischer BM, Walther M, Jepsen PU (2002) Far-infrared vibrational modes of DNA components studied by terahertz time-domain spectroscopy. Phys Med Biol 47:3807–3814
5. Bixon M, Jortner J (2001) Charge transport in DNA via thermally induced hopping. J Am Chem Soc 123:12556–12567
6. Szafran B, Adamowski J, Bednarek S (2000) Single-electron charging of self assembled quantum dots. Thin Solid Films 367:93–96
7. Porath D, Bezryadin A, Sd V, Dekker C (2000) Direct measurement of electrical transport through DNA molecules. Nature 403:635–638
8. Porath D, Bezryadin A, de Vries S, Dekker C (2000) Direct measurement of electrical transport through DNA molecules. Nature 403:635–638
9. Storhoff JJ, Mirkin CA (1999) Programmed Materials Synthesis with DNA. Chem Rev 99:1849–1862
10. Davies SW, Eizenman M, Pasupathy S (1999) Optimal structure for automatic processing of DNA sequences. IEEE Trans Biomed Eng 46:1044–1056
11. Fukui K, Tanaka K (1998) Distance dependence of photoinduced electron transfer in DNA. Angew Chem Int Ed 37:158–161
12. Smith DA, Ulmer CW II, Gilbert MJ (1992) Structural studies of aromatic amines and the DNA intercalating compounds m-amsa and o-amsa: Comparison of MNDO, AM1, and PM3 to experimental and ab initio results. J Comput Chem 13:640–650
13. Takada T, Kawai K, Fujitsuka M, Majima T (2004) Direct observation of hole transfer through double-helical DNA over 100 A. PNAS 101:14002–14006
14. Bobadilla AD, Bellido EP, Seminario JM (2009) Transmission of vibrational signals through a CNT-DNA interface In: Nanoelectronic devices for defense and security conference. Bahia Mar Beach Resort, Fort Lauderdale, FL
15. Bobadilla AD, Bellido EP, Rangel NL, Zhong H, Norton M, Sinitskii A, Seminario JM (2009) DNA origami impedance measurement at room temperature. J Chem Phys 130:171101
16. Bellido EP, Bobadilla AD, Rangel NL, Zhong H, Norton M, Sinitskii A, Seminario JM (2009) Current-voltage-temperature characteristics of DNA origami. Nanotechnology 20
17. Juarregui LA, Seminario JM (2008) A DNA sensor for sequencing and mismatches based on electron transport through Watson-Crick and non-Watson-Crick base pairs. IEEE Sensors 8:803–814
18. Jauregui LA, M. SJ (2008) Transversal Characteristics of DNA devices. Paper presented at the Nanotechnology, 2008. Nano-08. 8th IEEE Conference, 18-21 Aug 2008
19. Hong S, Jauregui LA, Rangel NL, Cao H, Day S, Norton ML, Sinitskii AS, Jorge M. Seminario (2008) Impedance measurements on a DNA junction. J Chem Phys 128:201103 (201101-201104)
20. Hv Z, Schiffrin DJ, Bates AD, Starikov EB, Wenzel W, Nichols RJ (2006) Variable-Temperature Measurements of the Single-Molecule Conductance of Double-Stranded DNA. Angew Chem Int Ed 45:5499–5502
21. Rangel NL, Sotelo JC, Seminario JM (2009) Mechanism of carbon-nanotubes unzipping into graphene ribbons. J Chem Phys 131:031105(031101-031104)
22. Marches R, Chakravarty P, Musselman IH, Bajaj P, Azad RN, Pantano P, Draper RK, Vitetta ES (2009) Specific thermal ablation of tumor cells using single-walled carbon nanotubes targeted by covalently-coupled monoclonal antibodies. Int J Cancer 125:2970–2977. doi:10.1002/ijc.24659
23. Agapito LA, Bautista EJ, Seminario JM (2007) Conductance model of gold-molecule-silicon and carbon nanotube-molecule-silicon junctions. Phys Rev B 76:115316(115311-115312)
24. Tour JM (2004) Functionalization of carbon nanotubes. Abstr Pap Am Chem Soc 227:U265–U265
25. Liang GC, Ghosh AW, Paulsson M, Datta S (2004) Electrostatic potential profiles of molecular conductors. Phys Rev B 69
26. Collins PG, Avouris P (2000) Nanotubes for Electronics. Scientific American (December)
27. Odom TW, Huang JL, Kim P, Lieber CM (1998) Atomic Structure and Electronic Properties of Single-Walled Carbon Nanotubes. Science 391:62
28. Tans SJ, Devoret MH, Dai H, Thess A, Richard ES, Geerligs LJ, Dekker C (1997) Individual Single-wall Carbon Nanotubes. Nature 386:474–477
29. Bockrath M, Cobden DH, McEuen PL, Chopra NG, Zettl A, Thess A, Smalley RE (1977) Single-electron transport in ropes of carbon nanotubes. Science 275:1922–1925
30. Pan BF, Cui DX, Xu P, Chen H, Liu FT, Li Q, Huang T, You XG, Shao J, Bao CC, Gao F, He R, Shu MJ, Ma YJ (2007) Design of dendrimer modified carbon nanotubes for gene delivery. Chinese J Cancer Res 19:1–6. doi:10.1007/s11670-007-0001-0
31. Krasheninnikov AV, Banhart F (2007) Engineering of nanostructured carbon materials with electron or ion beams. Nat Mater 6:723–733
32. Rothemund PWK (2006) Folding DNA to create nanoscale shapes and patterns. Nature 440:297–302. doi:10.1038/nature04586
33. Otero-Navas I, Seminario JM (2011) Molecular electrostatic potentials of DNA base-base pairing and mispairing. J Mol Model. doi:10.1007/s00894-011-1028-1
34. Jauregui LA, Salazar-Salinas K, Seminario JM (2009) Transverse electronic transport in double-stranded DNA nucleotides. J Phys Chem B 113:6230–6239
35. Kuzyk A, Yurke B, Toppari JJ, Linko V, Törmä P (2008) Dielectrophoretic trapping of DNA origami. Small 4:447–450
36. Linko V, Paasonen S-T, Kuzyk A, Törmä P, Toppari JJ (2009) Characterization of the Conductance Mechanisms of DNA Origami by AC Impedance Spectroscopy. Small 5:2382–2386
37. Tu X, Manohar S, Jagota A, Zheng M (2009) DNA sequence motifs for structure-specific recognition and separation of carbon nanotubes. Nature 460:250–253. doi:10.1038/nature08116
38. Maune HT, Han SP, Barish RD, Bockrath M, Goddard A II, Rothemund Paul WK, Winfree E (2010) Self-assembly of carbon nanotubes into two-dimensional geometries using DNA origami templates. Nat Nano 5:61–66. doi:10.1038/nnano.2009.311
39. Germarie SP et al (2007) DNA-mediated self-assembly of carbon nanotubes on gold. J Phys Conf Ser 61:1017

40. Li S, He P, Dong J, Guo Z, Dai L (2004) DNA-directed self-assembling of carbon nanotubes. J Am Chem Soc 127:14–15. doi:10.1021/ja0446045
41. Li Y, Han X, Deng Z (2007) Grafting single-walled carbon nanotubes with highly hybridizable DNA sequences: potential building blocks for DNA-programmed material assembly13. Angew Chem Int Ed 46:7481–7484
42. Seminario JM, Yan L (2005) Ab initio analysis of electron currents in thioalkanes. Int J Quantum Chem 102:711–723
43. Derosa PA, Guda S, Seminario JM (2003) A programmable molecular diode driven by charge-induced conformational changes. J Am Chem Soc 125:14240–14241
44. Seminario JM, De La Cruz C, Derosa PA, Yan L (2004) Nanometer-size conducting and insulating molecular devices. J Phys Chem B 108:17879–17885
45. Seminario JM, Araujo RA, Yan L (2004) Negative differential resistance in metallic and semiconducting clusters. J Phys Chem B 108:6915–6918
46. Seminario JM, Derosa PA, Cordova LE, Bozard BH (2004) A molecular device operating at terahertz frequencies. IEEE Trans Nanotech 3:215–218
47. Seminario JM, Yan L, Ma Y (2005) Scenarios for molecular-level signal processing. Proc IEEE 93:1753–1764
48. Johnson RR, Johnson ATC, Klein ML (2008) Probing the structure of DNA−carbon nanotube hybrids with molecular dynamics. Nano Lett 8:69–75. doi:10.1021/nl071909j
49. Johnson RR, Kohlmeyer A, Johnson ATC, Klein ML (2009) Free energy landscape of a DNA−carbon nanotube hybrid using replica exchange molecular dynamics. Nano Letters 9:537–541. doi:10.1021/nl802645d
50. Zheng M, Jagota A, Strano MS, Santos AP, Barone P, Chou SG, Diner BA, Dresselhaus MS, Mclean RS, Onoa GB, Samsonidze GG, Semke ED, Usrey M, Walls DJ (2003) Structure-based carbon nanotube sorting by sequence-dependent DNA assembly. Science 302:1545–1548. doi:10.1126/science.1091911
51. Guo X, Gorodetsky AA, Hone J, Barton JK, Nuckolls C (2008) Conductivity of a single DNA duplex bridging a carbon nanotube gap. Nat Nano 3:163–167. doi:10.1038/nnano.2008.4
52. Martínez L, Andrade R, Birgin EG, Martínez JM (2009) PACKMOL: a package for building initial configurations for molecular dynamics simulations. J Comput Chem 30:2157–2164
53. MacKerell AD, Bashford D, Bellott DRL, Evanseck JD, Field MJ, Fischer S, Gao J, Guo H, Ha S, Joseph-McCarthy D, Kuchnir L, Kuczera K, Lau FTK, Mattos C, Michnick S, Ngo T, Nguyen DT, Prodhom B, Reiher WE, Roux B, Schlenkrich M, Smith JC, Stote R, Straub J, Watanabe M, Wiorkiewicz-Kuczera J, Yin D, Karplus M (1998) All-atom empirical potential for molecular modeling and dynamics studies of proteins. J Phys Chem B 102:3586–3616. doi:10.1021/jp973084f
54. Plimpton S (1995) Fast Parallel Algorithms for Short-Range Molecular Dynamics. J Comput Phys 117:1–19
55. Hockney RW, Eastwood JW (1988) Computer simulation using particles. Taylor & Francis, New York
56. Berendsen HJC, Postma JPM, van Gunsteren WF, Dinola A, Haak JR (1984) Molecular dynamics with coupling to an external bath. J Chem Phys 81:3684–3690
57. Humphrey W, Dalke A, Schulten K (1996) VMD: visual molecular dynamics. J Mol Graphics 14:33–38